NCBI PubMed National Library of Medicine NLM
My NCBI [Sign In] [Register]
All Databases PubMed Nucleotide Protein Genome Structure OMIM PMC Journals Books
Search PubMed for Go Clear
Limits Preview/Index History Clipboard Details
Display Abstract Show: 20 Sort Send to Text
All: 1 Review: 0

About Entrez
Text Version

Entrez PubMed
Overview
Help | FAQ
Tutorial
New/Noteworthy
E-Utilities

PubMed Services
Journals Database
MeSH Database
Single Citation Matcher
Batch Citation Matcher
Clinical Queries
LinkOut
My NCBI (Cubby)

Related Resources
Order Documents
NLM Catalog
NLM Gateway
TOXNET
Consumer Health
Clinical Alerts
ClinicalTrials.gov
PubMed Central

☐1: Cardiovasc Intervent Radiol. 2004 May-Jun;27(3):288-90. Related Articles, Links

A case of aorto-bronchial fistula after insertion of left main bronchial self-expanding metallic stent in a patient with recurrent esophageal cancer.

Onishi H, Kuriyama K, Komiyama T, Tanaka S, Marino K, Tsukamoto T, Araki T.

Department of Radiation Oncology, Yamanashi Medical University, 1110 Shimokato Tamaho-cho Nakakoma-gun Yamanashi, 409-3898, Japan. honishi@res.yamanashi-med.ac.jp

We report a case of aorto-bronchial fistula (ABF) caused by a self expanding metallic stent (EMS) 51 days after insertion into the left main bronchus. The patient presented with left main bronchial stenosis caused by post-operative local recurrence of esophageal cancer. Post-operative radio therapy totaling 40 Gy and post-recurrence radiotherapy totaling 34 Gy were administered, with daily fractions of 2 Gy. Stenosis of the left main bronchus improved slightly, and was followed with insertion of EMS to prevent restenosis. The patient experienced massive hemoptysis for 3 days before sudden death. Autopsy revealed the EMS edge perforating the descending aortic lumen. Tumor infiltration and bacterial infection were observed on the wall of the left bronchus, and atherosclerosis was present on the aortic wall around the fistula. It should be noted that the left main bronchus was at considerable risk of ABF after insertion of EMS for malignant stenosis, and prophylactic sent insertion into the left bronchus without imperative need must be avoided.

Publication Types:
- Case Reports

PMID: 15359474 [PubMed - indexed for MEDLINE]

Display Abstract Show: 20 Sort Send to Text

Write to the Help Desk
NCBI | NLM | NIH
Department of Health & Human Services
Privacy Statement | Freedom of Information Act | Disclaimer

Mar 6 2005 07:57:22

Radiation Injury After Hypofractionated Stereotactic Radiotherapy for Peripheral Small Lung Tumors: Serial Changes on CT

Toshiaki Takeda[1]
Atsuya Takeda[1]
Etsuo Kunieda[1,2]
Akitoshi Ishizaka[3]
Kazuhiko Takemasa[1]
Kyoko Shimada[1]
Seika Yamamoto[1]
Naoyuki Shigematsu[2]
Osamu Kawaguchi[2]
Jun-ichi Fukada[1,2]
Toshio Ohashi[2]
Sachio Kuribayashi[2]
Atsushi Kubo[2]

OBJECTIVE. We studied the serial changes and CT manifestations of pulmonary radiation injury after hypofractionated stereotactic radiation therapy for peripheral small lung tumors.

SUBJECTS AND METHODS. Hypofractionated stereotactic radiation therapy was applied to 20 patients with proven primary ($n = 11$) or metastatic ($n = 9$) lung cancer, for a total of 22 lesions of 3 cm or less in diameter located within 3 cm from the parietal pleural surface. Follow-up CT was scheduled at 1 and 3 months, and every 3 months thereafter.

RESULTS. Ground-glass opacities were observed around four (18%) of 22 lesions at 3–6 months. The opacities nearly corresponded to the planned target volume, but half of them were unevenly distributed. Ground-glass opacities gradually disappeared or evolved into dense consolidation while shrinking. Dense consolidations developed in 16 (73%) of 22 lesions, including seven in the center of the planned target volume and nine in the periphery of the planned target volume. Dense consolidations moved in six of these 16 lesions and gradually shrank, becoming fixed as solid or linear opacities approximately 12 months later.

CONCLUSION. The pulmonary opacities observed after hypofractionated stereotactic radiation therapy for peripheral small lung tumors may not precisely correspond to the planned target volume (unlike those with conventional radiation therapy) and may change in shape and location dynamically during the first year. Knowledge of these findings is necessary to avoid misunderstandings concerning tumor regrowth or new tumors.

Currently, surgery is the treatment of choice in the early stages of lung cancer. Although conventional radiation therapy may be selected as a less invasive intervention in elderly patients and in those with inoperable disease, the rate of local control of malignancy after radiation therapy is approximately 30%, which is lower than for surgical resection [1]. Stereotactic irradiation can deliver high radiation doses to localized lesions with great accuracy, allowing a strong antitumoral effect while lessening radiation injury to normal tissues [2]; it has been applied to the treatment of small intracranial tumors with excellent results [2]. More recently, hypofractionated stereotactic radiotherapy has been applied to the treatment of extracranial malignant tumors, with preliminary studies reporting greater than 90% control rates for small localized lung tumors [3–5].

In this study, we applied hypofractionated stereotactic radiotherapy to the treatment of small lung tumors and observed the various radiologic patterns of change after irradiation. As indicated by previous reports [6, 7], radiation injuries caused by conventional coplanar radiotherapy show distinct linear margins on CT that correspond to the margins of the irradiation field. However, because hypofractionated stereotactic radiotherapy is delivered in a 3D spherical volume with a steep gradient between the periphery of the planned target volume and normal adjacent tissue, the shape of the radiation injury should be considered three-dimensionally. Hypofractionated high-dose irradiation, with highly concentrated narrow beams that target small volumes, is associated with markedly different dose distributions and biologic effects on tissues from those described for coplanar conventional radiotherapy. The aim of this study was to describe the CT characteristics of radiation injury after hypofractionated stereotactic radiotherapy for small lung malignancies.

Subjects and Methods

The patient population consisted of 17 men and three women (age range, 56–89 years; median, 72.6

Received June 16, 2003; accepted after revision November 10, 2003.

[1]Department of Radiology, Tokyo Metropolitan Hiro-o General Hospital, 2-34-10 Ebisu, Shibuya-ku, Tokyo 150-0013, Japan. Address correspondence to T. Takeda (t-takeda@hiroo-hospital.metro.tokyo.jp).

[2]Department of Radiology, School of Medicine, Keio University, 35 Shinanomachi, Shinkuku-ku, Tokyo 160-8582, Japan.

[3]Department of Medicine, School of Medicine, Keio University, Tokyo 160-8582, Japan.

AJR 2004;182:1123–1128

0361–803X/04/1825–1123

© American Roentgen Ray Society

years) who were treated with hypofractionated stereotactic radiotherapy at our institutions between January 1998 and November 2002. For most patients, surgery was not indicated because of patient age, the presence of multiple lesions, or poor pulmonary function. Five patients preferred hypofractionated stereotactic radiotherapy treatment even though surgery was possible. The study protocol was approved by the institutional review boards of the institutions, and written informed consent was obtained from each participant before hypofractionated stereotactic radiotherapy was performed.

Primary lung cancer was pathologically proven in 11 patients (11 lesions), and metastases from other primary cancers were diagnosed clinically in nine patients (11 lesions). Hypofractionated stereotactic radiotherapy was generally considered if the tumor was 3 cm or smaller in diameter, if it was 3 cm or less from the parietal pleural surface, if craniocaudal breathing-associated motion of the lesion was 1 cm or less, and if three or fewer lesions were present at the start of treatment. Because the risk of atelectasis and reduction of pulmonary function caused by the collapse of large bronchi was unknown, potential lesions for treatment were limited to peripheral lesions 3 cm or less from the parietal pleural surface so that the planned target volume would not contain lobar bronchi. Tumor pathology and mean tumor volumes are listed in Table 1.

Pretreatment Evaluation and Radiation Treatment

The planned target volume was determined using CT (Xvision, Toshiba) performed on patients who were breathing at rest. Serial 2-mm-thick scans were obtained in 2-mm increments at 4–8 sec per slice. Longer scanning periods were used to define the tumor trajectory associated with breathing. The planned target volume consisted of the imaged volume, defined as the gross tumor volume plus an internal margin, plus a 5- to 10-mm setup margin.

Tumor volumes (V) were calculated according to the following formula:

$$V = 4/3\,\pi \times R_1 \times R_2 \times R_3,$$

where R_1 (half the maximum diameter), R_2 (half the diameter perpendicular to R_1), and R_3 (half the maximum diameter in the craniocaudal direction) were obtained with calipers on CT. When the tumor margin was ill defined, the outermost circumference was used. The diameter in the craniocaudal direction was defined as the product of the thickness and the number of slices from the top to the bottom of the lesion. Estimated tumor volumes ranged from 0.5 to 45.5 cm^3 (mean, 9.5 cm^3).

Treatments were planned using a radiation treatment planning system (FOCUS version 2.7.0, Computerized Medical Systems). Volumes to be treated were set so that the planned target volume received an 80% isodose of the maximum dose, with 80% isodose defined as the therapeutic dose (Figs. 1A, 2A, and 3A). The shape of the field was adjusted dynamically according to the tumor shape using a multileaf collimator.

The irradiation dose generally consisted of 50 Gy in five fractions administered over 5–7 days. Seventeen lesions in 15 patients were treated using this dose regimen. When a tumor was adjacent to critical organs (e.g., spinal cord or esophagus), the fractionated dose was reduced to 5–7 Gy and the total dose was limited to 40–50 Gy.

Radiologic Follow-Up

Patients were interviewed monthly to determine the presence or absence of symptoms and for chest roentgenographic examination.

TABLE 1 CT Manifestations of Radiation Pneumonitis

Lesion Characteristics			Ground-Glass Opacity		Dense Consolidation					Bronchiectasis
No.	Pathology	Volume (cm^3)[a]	Time of Appearance (mo)	Distribution	Time of Appearance (mo)[c]	Location[b]	Shrinkage (mo)[c]	Movement	Fixation (mo)[c]	Time of Appearance (mo)
1	Metastasis	0.5	—		4	Center	8	Hilum	11	8
2	Metastasis	4.7	—		8	Center	11	Pleura	—	4
3	Metastasis	25.6	—		3	Periphery	9	Hilum	12	6
4	Metastasis	6.3	—		6	Center	9	Hilum	12	6
5	Squamous cell carcinoma	15.1	—		5	Center	—	—	—	—
6	Adenocarcinoma	—	—		—		—	—	—	—
7	Metastasis	1.1	6	Even	—		—	—	—	—
8	Squamous cell carcinoma	12.7	4–6	Even	6	Center	9	Hilum	12	6
9	Metastasis	3.6	4–6	Uneven	6	Center	9	—	—	6
10	Adenocarcinoma	10.3	—		3	Periphery	—	Hilum	—	6
11	Squamous cell carcinoma	11.2	—		3	Periphery	—	—	—	3
12	Adenocarcinoma	26.6	—		—		—	—	—	—
13	Metastasis	3.1	—		5	Periphery	—	—	9	—
14	Metastasis	8.2	—		4	Center	—	—	—	4
15	Metastasis	0.9	—		3	Periphery	6	—	6	5
16	Metastasis	0.5	—		—		—	—	—	—
17	Squamous cell carcinoma	—	—		—		—	—	—	—
18	Adenocarcinoma	2.8	—		6	Periphery	—	—	—	—
19	Adenocarcinoma	7.9	—		3	Periphery	—	—	—	—
20	Adenocarcinoma	0.7	—		3	Periphery	—	—	—	—
21	Metastasis	2.0	3	Uneven	4	Periphery	—	—	—	—
22	Squamous cell carcinoma	45.5	—		—		—	—	—	—

Note.—Dash (—) indicates changes were not observed.

[a]Estimated. Volumes of lesions 6 and 17 were not calculated because they were postoperative residual tumors already enclosed in scars.

[b]Center of planned target volume or periphery of planned target volume.

[c]First observed after therapy.

Lesion characteristics were periodically examined on CT (Xvigor or Xvision, Toshiba) even in the absence of clinical symptoms at follow-up visits approximately 1 and 3 months after treatment, and in principle every 3 months thereafter. The interval of CT varied slightly depending on each patient's clinical status. If dubious opacities were seen on periodic radiography, additional CT was performed between the scheduled examinations. Single-slice helical CT of the entire lung without contrast material was performed using scanning parameters of slice thickness, 10 mm; pitch, 1; tube voltage, 120 kV; tube current, 200 mA; and 0.75 sec per slice. Images focused on tumors and associated pneumonitis were obtained by helical scanning with slice thickness, 2 mm; pitch, 1; tube voltage, 120 kV; tube current, 250 mA; and 0.75 sec per slice. High-resolution CT was reconstructed using a high-spatial-resolution algorithm. Of 100 total CT series, high-resolution CT scans were obtained concurrently in 61 studies. An average of 4.5 CT series per lesion were performed, including an average of 2.8 high-resolution CT series. The mean follow-up period after high-resolution CT was 17.6 months (range, 4.5–51.6 months). No patients received chemotherapy.

Interpretation of CT Findings

The time of appearance of ground-glass opacities or dense consolidations (with respect to completion of radiation therapy), location of appearance (center or periphery of the planned target volume), serial changes (changes in density, size, and location), and time of appearance of bronchiectasis were systematically recorded. CT images were independently interpreted by four diagnostic radiologists who were familiar with the clinical diagnosis and the development of lung tumors. CT characteristics were determined on the basis of a consensus among at least three of the four examiners.

Results

Demographic characteristics of the lesions and characteristics of the radiation injuries are detailed in Table 1.

After hypofractionated stereotactic radiotherapy, ground-glass opacities and dense consolidations were observed as initial lung CT findings at 3–4 months. Thereafter, the ground-glass opacities either disappeared or evolved into dense consolidations. Dense consolidations that were seen initially gradually shrank to become solid or linear opacities con-

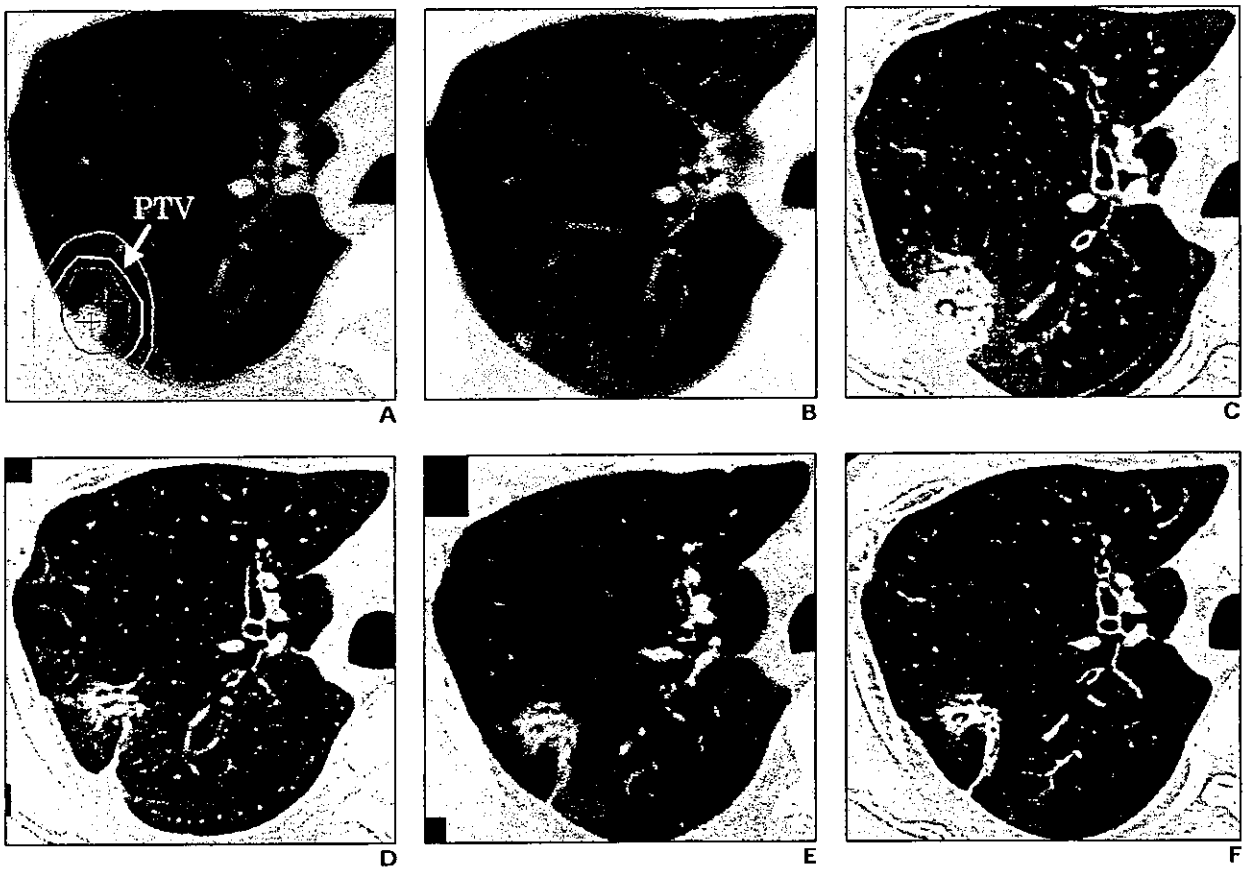

Fig. 1.—59-year-old man with lung metastasis from rectal carcinoma. Typical characteristics of radiation pneumonitis and fibrosis after hypofractionated stereotactic radiotherapy are seen on serial lung CT scans after irradiation.
A, Axial unenhanced CT scan obtained before treatment shows tumor in right upper lobe. PTV = planned target volume.
B, CT scan at 1 month after irradiation shows decrease in tumor size.
C, CT scan at 4 months reveals appearance of dense consolidation and its surrounding ground-glass opacity.
D, CT scan at 8 months shows shrinkage of dense consolidation and its movement toward hilum.
E, CT scan at 11 months shows presence of dilated bronchi within opacity.
F, CT scan at 22 months shows fixation of opacity. Subsequent CT characteristics remained unchanged.

sistent with lesion fixation (Figs. 1–3). No ground-glass opacities or dense consolidations were observed at sites remote from the planned target volume.

Ground-glass opacities appeared on CT scans in four (18%) of 22 lesions at 3–6 months after completion of radiation therapy. They all corresponded closely to the planned target volume. In two instances, the ground-glass opacities were evenly distributed in the planned target volume (Figs. 1C and 3C), and in the other two instances the opacities remained unevenly distributed at 4 months, thereafter evolving into dense consolidations consistent with the planned target volume.

Dense consolidations appeared in 16 (73%) of 22 lesions on CT scans obtained at 3- to 8-months' follow-up. Of these, seven exhibited dense peritumoral consolidations corresponding to the planned target volume (Figs. 1C and 2D), and the remaining nine showed consolidation limited to the margin of the planned target volume, a short distance from the isocenter (Figs. 3C and 3D). Although dense consolidations shrank in seven (44%) of these 16 lesions, the consolidations did not disappear completely but persisted as solid or linear opacities (Figs. 1F, 2E, and 3F). This shrinkage occurred within 6–11 months after radiotherapy. In six of 10 lesions followed up for at least 12 months, the pulmonary opacities became fixed on CT scans, consistent with the development of fibrosis. Movement of the opacity was observed in six (37.5%) of the 16 densely consolidated lesions. This movement was detected simultaneously with shrinkage in five of the six lesions, with movement toward the hilum in five (Figs. 1 and 2A–2D), and with movement away from the hilum in one.

Bronchiectasis was present in 10 (45.5%) of 22 lesions and developed almost contemporaneously with dense consolidations that contained dilated or thickened bronchi. Bronchial thickening and lumen irregularities caused by traction (i.e., traction bronchiectasis) became apparent along with movement of the opacities (Figs. 2D and 3E).

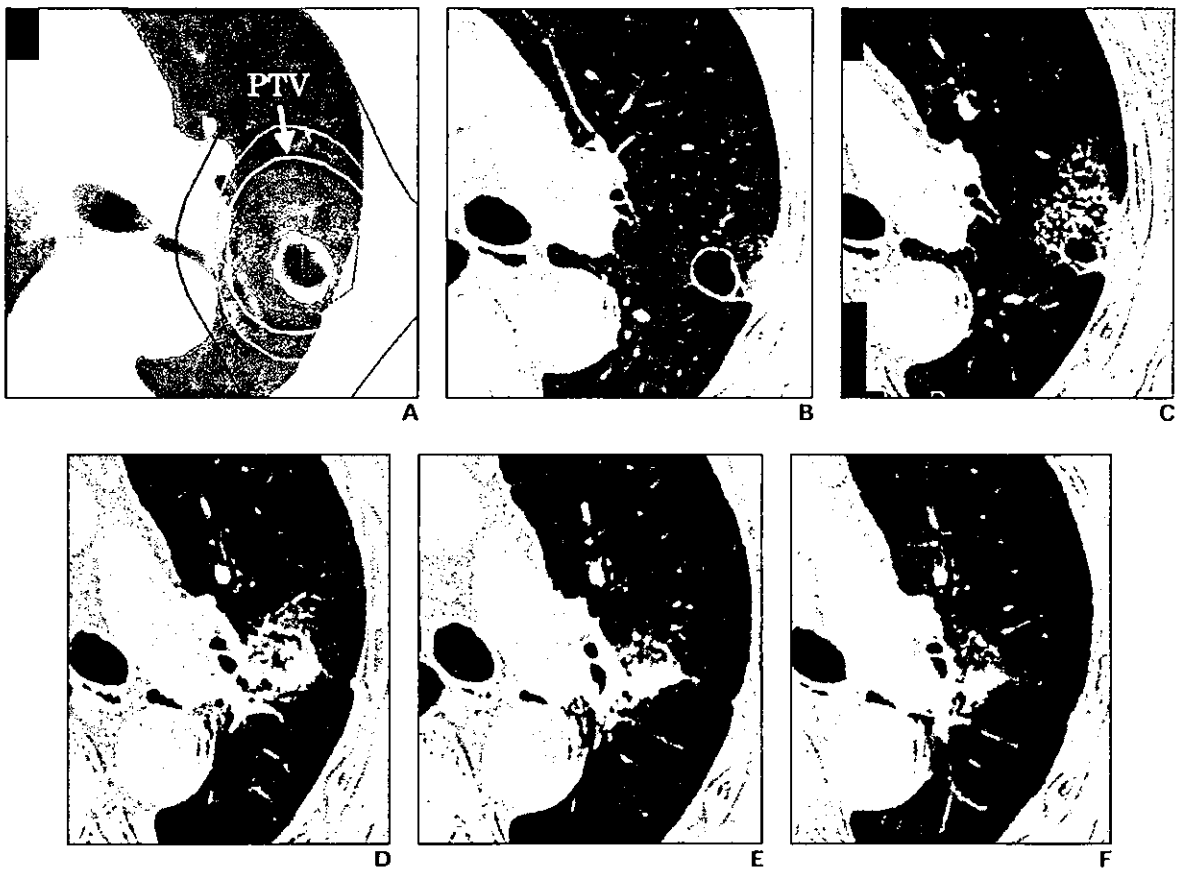

Fig. 2.—85-year-old man with squamous cell cancer.
A, Axial unenhanced CT scan obtained before treatment shows cavitated tumor in left upper lobe. PTV = planned target volume.
B, CT scan at 1 month after irradiation shows almost no change.
C, CT scan at 4 months shows presence of ground-glass opacity distributed in planned target volume.
D, CT scan at 6 months shows conversion of ground-glass opacity to dense consolidation and shift toward hilum. Tumor has almost disappeared.
E, CT scan at 10 months shows shrinkage of opacity and further movement toward hilum.
F, CT scan at 12 months shows further decrease in size. Subsequently, opacity remained unchanged.

Discussion

Hypofractionated stereotactic radiotherapy, a new treatment method for small lung malignancies, differs considerably from conventional coplanar radiation therapy because it consists of delivering a single high dose of radiation with hypofractionation to small irradiation fields. Although hypofractionated stereotactic radiotherapy is expected to be highly effective in the control of localized lesions, its acceptance and indications will expand only if its use is not complicated by high rates of adverse reactions. Therefore, before considering increased radiation doses in the hope of achieving improved local therapeutic effects, a thorough clinical and radiologic evaluation of pulmonary parenchymal injuries caused by irradiation is needed to verify that hypofractionated stereotactic radiotherapy is a safe and effective treatment for small lung malignancies.

Classic radiation pneumonitis induced by conventional radiation therapy is characterized by a linear margin demarcating the treatment port and is uncommon with exposures of less than 30 Gy but inevitable for exposures greater than 40 Gy [8]. However, the reported incidence of clinical manifestations associated with radiation pneumonitis is 7–8%, and the symptoms are usually mild, despite imaging findings that may appear more prominent [9, 10]. In our study, only three patients reported a mild cough associated with radiation injury, and all were successfully treated with simple therapy. In contrast, sporadic radiation pneumonitis is an immune-mediated process resulting in lymphocytic alveolitis that leads to a response remote from the localized pulmonary irradiation and that is usually associated with severe symptoms and high mortality in the absence of a "threshold" dose [11]. Classic radiation pneumonitis can be classified as either early (1–3 months after irradiation) or late (3–6 months after irradiation), depending on the time of appearance of the pulmonary reaction to the radiation. In our study, hypofractionated stereotactic radiotherapy-induced lung injuries did not systematically develop in the center of treated volumes, but often began at the periphery. However, injuries eventually conformed to and remained in the planned target

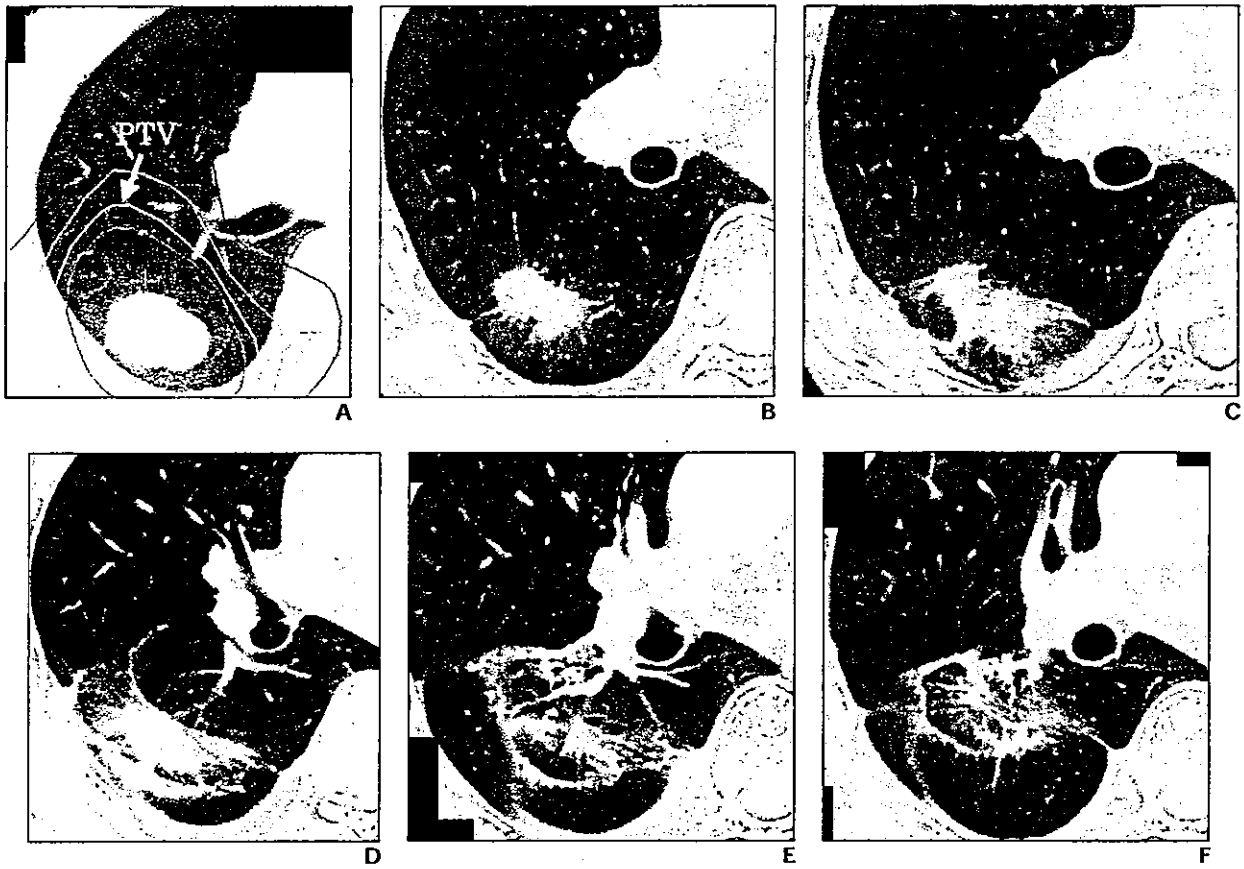

Fig. 3.—70-year-old man with lung metastasis of oropharyngeal carcinoma.
A, Axial unenhanced CT scan obtained before treatment shows metastatic tumor in right lower lobe. PTV = planned target volume.
B, CT scan at 1 month after irradiation shows decrease in tumor size.
C, CT scan at 3 months reveals appearance of dense consolidation in subpleural space of planned target volume.
D, CT scan at 6 months shows increase in size of dense consolidation and onset of movement. Center of tumor is now located more cranially.
E, CT scan at 9 months shows decrease in tumor size, thinning of dense consolidation, and movement of lesion toward hilum.
F, CT scan at 12 months shows presence of linear opacity surrounding tumor and fixation of lesion.

volume. These findings suggested that a threshold dose was required to develop pneumonitis, and that hypofractionated stereotactic radiotherapy-induced lung injuries were classifiable as classic radiation pneumonitis.

Evolution from ground-glass opacity to dense consolidation to fibrosis was observed on CT in a relatively small subset of our patients. In contrast, in a study of 3D conformal radiation therapy, Koenig et al. [12] observed the development of ground-glass opacity around tumors on CT scans at 3 months after radiation therapy in 19 of 19 patients treated with total doses between 69.6 and 90.3 Gy in 33–58 fractions. Three-dimensional conformal radiation therapy used in that study differs considerably from the hypofractionated stereotactic radiotherapy used in our study, particularly from the standpoint of the single dose. The incidence and severity of radiation pneumonitis can depend on the extent of irradiation, the total dose, and the number of fractions, and may also be influenced by concurrent chemotherapy [9]. Thus, the differences between the two studies with regard to CT patterns are probably attributable to researchers for the previous study using a higher radiation dose delivered as a single fraction. Therefore, we hypothesize that on CT, early or mild radiation injuries appear as ground-glass opacities, whereas severe radiation injuries appear as dense consolidations.

Movement of dense consolidations often occurred. Movement toward the hilum was seen in all but one case. Because shrinkage of the opacity and traction bronchiectasis were usually seen concurrently, the mechanism of these phenomena seems attributable to fibrosis. Therefore, we think that the apparent movement of the opacity is largely attributable to the deformity of the lung caused by fibrosis. Takahashi et al. [13] observed that the ground-glass opacities corresponded to thickened interlobular walls because of fibroblastic cells and collagen fibers in a pig model of radiation pneumonitis.

Takahashi et al. [13] also found that the ground-glass opacities were not evenly distributed but at pathology were predominant near the interstitium. In a dog model, the same radiation dose caused a more severe reaction when delivered to the periphery of the right lower lobe than to the right hilum [14]. These findings indicate that variable local sensitivity to radiation, depending on the amount of interstitium, causes nonuniform distribution of ground-glass opacities and dense consolidations.

We acknowledge several limitations in our study. Although we differentiated radiation injury patterns as ground-glass opacity, dense consolidation, and fibrosis, we had no pathologic proof. As with other studies examining radiation pneumonitis, we found it difficult to obtain specimens from otherwise asymptomatic patients. Another limitation was the relatively small number of patients in our study. Although it is fortunate that only a few patients complained of mild cough and recovered without resorting to steroids or hospital admission, the number of patients was too small to allow analysis of the relationship among symptomatic pneumonitis, patient background factors, and radiation treatment.

In assessing radiologic findings, residual tumor regrowth, lymphatic spread, and infection should be differentiated from radiation pneumonitis. Local recurrences especially are sometimes difficult to diagnose in the early phase because they are often asymptomatic, as is radiation pneumonitis. Four cases recurred after hypofractionated stereotactic radiotherapy, of which two had no radiation pneumonitis–induced opacities and one had minimal ground-glass opacity. In these three cases, the initial radiation effect was minimal or could not be evaluated and tumors gradually enlarged without a dramatic change in shape. Therefore, regrowth of the tumors was readily diagnosed. In the last case, the tumor had almost disappeared shortly after hypofractionated stereotactic radiotherapy. Dense consolidation surrounding the initial tumor appeared 6 months later, followed by overtly solid tumor on its periphery. Needle biopsy confirmed the presence of adenocarcinoma. We suppose that this may be a typical case of recurrence after hypofractionated stereotactic radiotherapy. However, we have experienced too few cases to draw a clear-cut distinction between recurrence and radiation pneumonitis. It is important to be especially careful during the early assessment of radiation pneumonitis on CT because the CT pattern evolves serially, and pulmonary opacity can move. We should be aware that the CT appearance reflects only one phase of the spectrum.

In conclusion, a size decrease in small lung tumors was generally observable on CT scans 1–3 months after completion of irradiation by hypofractionated stereotactic radiotherapy. This decrease in tumor size was accompanied by reduced areas of dense consolidation and surrounding ground-glass opacity at 3–6 months. Although ground-glass opacities generally resolved, the dense consolidations assumed typical CT patterns, including movement toward the hilum, shrinkage, and fixation at approximately 1 year after treatment. The incidence of ground-glass opacities was relatively low, and neither ground-glass opacities nor dense consolidations coincided exactly with dose distribution, occasionally developing away from the isocenter or remaining heterogeneous. Dynamic changes in ground-glass opacities and dense consolidations were observed over time. Our results indicate that assessment of lesions should be done with knowledge of these changes of radiation pneumonitis on CT during the first year after treatment, before fixation, to avoid misunderstandings about CT findings resembling tumor regrowth or the appearance of new lesions.

References

1. Sibley GS. Radiotherapy for patients with medically inoperable stage I nonsmall cell lung carcinoma: smaller volumes and higher doses—a review. *Cancer* 1998;82:433–438
2. Wasserman TH, Rich KM, Drzymala RE, Simpson JR. Stereotactic irradiation. In: Perez CA, Brady LW, eds. *Principles and practice of radiation oncology*, 3rd ed. Philadelphia, PA: Lippincott-Raven, 1998:387–404
3. Fukumoto S, Shirato H, Shimizu S, et al. Small-volume image-guided radiotherapy using hypofractionated, coplanar, and noncoplanar multiple fields for patients with inoperable stage I nonsmall cell lung carcinomas. *Cancer* 2002;95: 1546–1553
4. Uematsu M, Shioda A, Tahara K, et al. Focal, high dose, and fractionated modified stereotactic radiation therapy for lung carcinoma patients: a preliminary experience. *Cancer* 1998;82:1062–1070.
5. Nagata Y, Negoro Y, Aoki T, et al. Clinical outcomes of 3D conformal hypofractionated single high-dose radiotherapy for one or two lung tumors using a stereotactic body frame. *Int J Radiat Oncol Biol Phys* 2002;52:1041–1046
6. Libshitz HI, Shuman LS. Radiation-induced pulmonary change: CT findings. *J Comput Assist Tomogr* 1984;8:15–19
7. Forrest LJ, Mahler PA, Vail DM, Mackie TR, Ladd WM, Kinsella TJ. Computed tomographic evaluation of radiation pneumonitis in a canine model. *Radiat Oncol Investig* 1998;6:128–134
8. Libshitz HI, Southard ME. Complications of radiation therapy: the thorax. *Semin Roentgenol* 1974;9:41–49
9. Movsas B, Raffin TA, Epstein AH, Link CJ Jr. Pulmonary radiation injury. *Chest* 1997;111: 1061–1076
10. Roach M III, Gandara DR, Yuo HS, et al. Radiation pneumonitis following combined modality therapy for lung cancer: analysis of prognostic factors. *J Clin Oncol* 1995;13:2606–2612
11. Morgan GW, Breit SN. Radiation and the lung: a reevaluation of the mechanisms mediating pulmonary injury. *Int J Radiat Oncol Biol Phys* 1995;31:361–369
12. Koenig TR, Munden RF, Erasmus JJ, et al. Radiation injury of the lung after three-dimensional conformal radiation therapy. *AJR* 2002;178: 1383–1388
13. Takahashi M, Balazs G, Pipman Y, et al. Radiation-induced lung injury using a pig model: evaluation by high-resolution computed tomography. *Invest Radiol* 1995;30:79–86
14. Stenton CG, Boland J. Experimental radiation pneumonitis: radiographic and pathologic correlation. *Cancer* 1967;20:2170–2183

Int. J. Radiation Oncology Biol. Phys., Vol. 58, No. 4, pp. 1280–1288, 2004
Copyright © 2004 Elsevier Inc.
Printed in the USA. All rights reserved
0360-3016/04/$–see front matter

ELSEVIER

doi:10.1016/j.ijrob.2003.10.010

PHYSICS CONTRIBUTION

EVALUATION OF NOVEL MODIFIED TANGENTIAL IRRADIATION TECHNIQUE FOR BREAST CANCER PATIENTS USING DOSE–VOLUME HISTOGRAMS

ATSUYA TAKEDA, M.D.,*† NAOYUKI SHIGEMATSU, M.D.,* TADASHI IKEDA, M.D.,‡ OSAMU KAWAGUCHI, M.D.,* SHOJI KUTSUKI, M.D.,* RYOCHI ISHIBASHI, M.D.,* ETSUO KUNIEDA, M.D.,* TOSHIAKI TAKEDA, M.D.,† KAZUHIKO TAKEMASA, M.D.,† HISAO ITO, M.D.,§ TAKASHI UNO, M.D.,§ HIROMITSU JINNO, M.D.,‡ AND ATSUSHI KUBO, M.D.*

Departments of *Radiology and ‡Surgery, Keio University School of Medicine, Shinjuku-ku, Tokyo, Japan; †Department of Radiology, Tokyo Metropolitan Hiroo Hospital, Shibuya-ku, Tokyo, Japan; §Department of Radiology, Chiba University School of Medicine, Inohana-ku, Chiba, Japan

Purpose: We have previously reported that entire axillary lymph node regions could be irradiated by the modified tangential irradiation technique (MTIT). In this study, MTIT was compared with a conventional irradiation technique (CTIT) using dose–volume histograms to verify how adequately MTIT covers the breast and axillary lymph node region and the extent to which it involves the lung and heart.

Methods and Materials: Forty-four patients with early-stage breast cancer were treated by lumpectomy, axillary dissection, and postoperative radiotherapy. Twenty-two patients were treated with MTIT and 22 with CTIT. In 25 patients, the breast tumor was on the left and in 19 on the right. During axillary dissection, surgical clips were left as markers at the border of the axillary lymph node region. MTIT was planned by setting the dorsal edge of the radiation field on a lateral-view simulator film at the dorsal edge of the humeral head and the cranial edge of the radiation field at the caudal edge of the humeral head. CTIT was planned to ensure radiation of the breast tissue without considering the axillary region. In this study, all patients underwent computed tomography, and the CT data were transmitted on-line to a radiotherapy planning system, in which the dose-distribution computed tomography images and dose–volume histograms were calculated by defining the breast, axillary region (levels I, II, and III), lung, and heart region.

Results: Dose–volume histogram analysis demonstrated that breast tissue was radiated with an 86.5–100% volume (median 96.5%) by MTIT and an 83–100% volume (median, 95%) by CTIT at >95% of the isocenter dose. The axillary lymph node regions at Levels I, II, and III were irradiated with 84–100% (median, 94.5%), 59–100% (median, 89%), and 70–100% (median, 89.5%) volumes, respectively, by MTIT and with 2–84% (median, 38%), 0–53% (median, 15%), and 0–31% (median, 0%) volumes, respectively, by CTIT at >70% of the isocenter dose. The ipsilateral lung was irradiated with a 5–22% volume (median, 11.5%) by MTIT and 5–15% volume (median 9%) by CTIT at >90% of the isocenter dose. In all 25 left-sided breast cancer patients, the volumes irradiated with an 80% isocenter dose were <30 cm^3.

Conclusion: The results of our study demonstrated that the breast tissue was sufficiently irradiated with both CTIT and MTIT planning, the axillary lymph node areas irradiated by MTIT were much wider than those irradiated by CTIT at all levels, and the lung and heart volumes irradiated by MTIT were small. © 2004 Elsevier Inc.

Breast cancer, Modified tangential irradiation technique, Axillary lymph nodes, Dose–volume histogram analysis.

INTRODUCTION

The role of routine axillary dissection is controversial in the management of localized breast cancer (1–3), and the option to perform axillary radiotherapy (RT) without axillary dissection or with only sentinel node biopsy is only available for clinically node-negative patients (4–10). Recently, three-dimensional conformal tangential RT and intensity-modulated RT using computed tomography (CT)-based three-dimensional treatment planning have been applied (11, 12) in an effort to improve the local control rate and reduce toxicity. However, many

Reprint requests to: Naoyuki Shigematsu, M.D. Department of Radiology, Keio University School of Medicine, 35 Shinanomachi, Shinjuku-ku, Tokyo 160-8582 Japan. Tel: (+81) 3-5363-3835; Fax: (+81) 3-3359-7425; E-mail: shige@rad.med.keio.ac.jp

Supported in part by a grant from Tokyo Ri-Igaku Kenkyujo, Japan.

Received Mar 10, 2003, and in revised form Sep 26, 2003. Accepted for publication Oct 15, 2003.

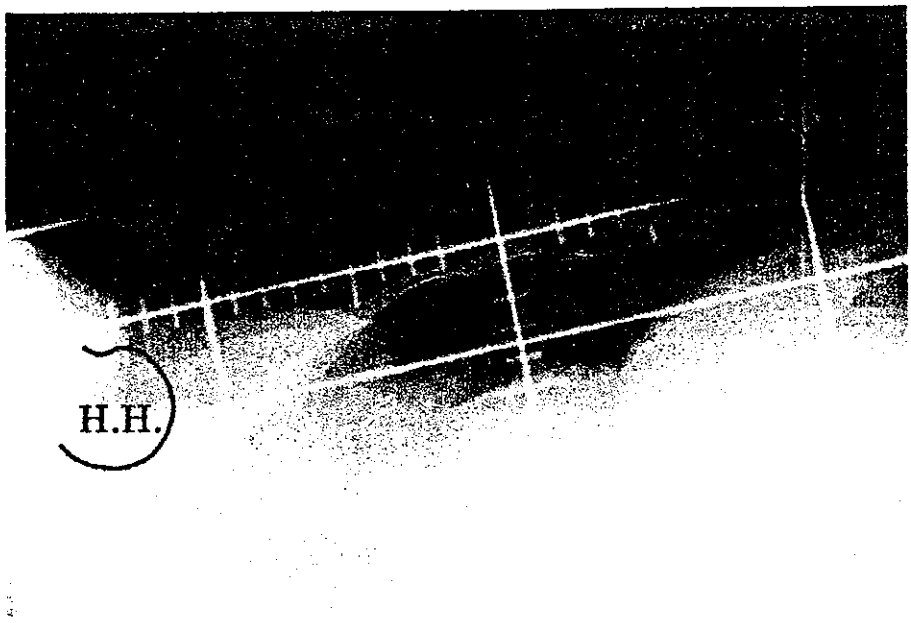

(a)

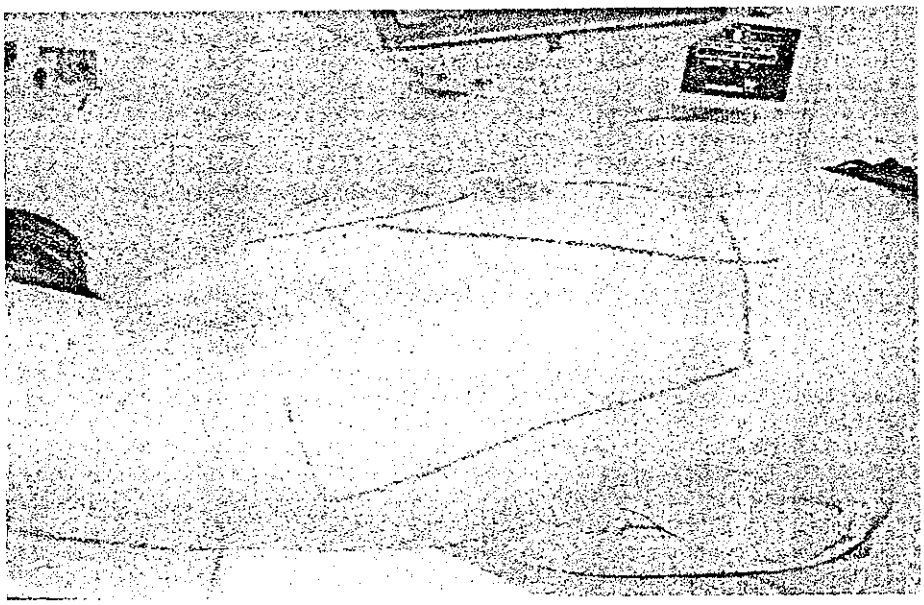

(b)

Fig. 1. Simulation films (anterior oblique view) and photographs of patients treated with (a,b) conventional irradiation technique and (c,d) modified tangential irradiation technique (MITT). In treatment with MTIT, field size tends to be wider in caudal and posterior directions and collimator and gantry angles tend to be deeper. Field from the anterior oblique view covers one-half of humeral head. H.H. = humeral head.

patients still undergo fluoroscopic simulation or planning without three-dimensional data (13), and coverage of the axillary lymph node region and involved lung and heart volumes by two-dimensional planning remains controversial (13, 14). As we previously reported, it is possible to irradiate almost the entire axillary lymph node region using the modified tangential irradiation technique (MTIT) (15). In this study, MTIT was compared with a conventional tangential irradiation technique (CTIT) using dose–volume histograms (DVHs) to verify how adequately MTIT covers the breast and axillary lymph node region and to estimate the extent of lung and heart RT.

METHODS AND MATERIALS

Between October 2000 and July 2001, 44 patients with early-stage breast cancer were treated by lumpectomy and axillary dissection at the Department of Surgery, Keio Uni-

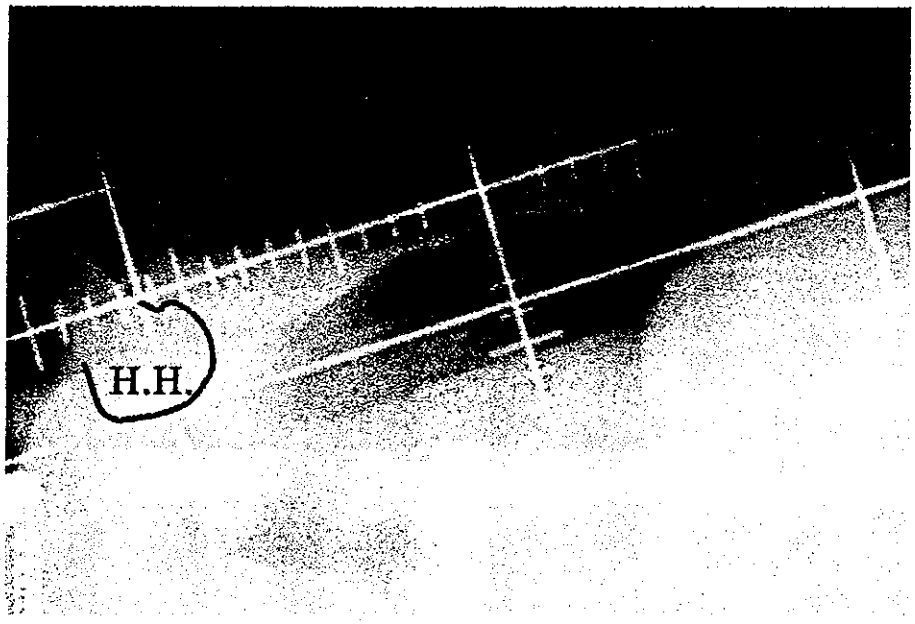

(c)

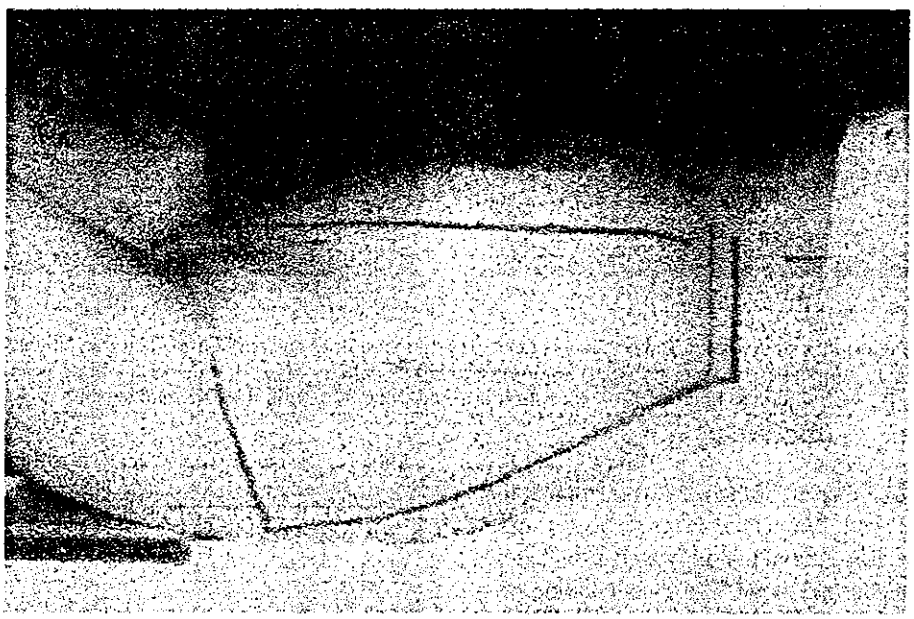

(d)

Fig. 1. *(Cont'd)*

versity Hospital. During axillary dissection, surgical clips were left as markers at the following sites: in the chest wall under the pectoralis minor muscle at the level of the axillary vein; immediately adjacent to the subscapular vein; in the latissimus dorsi muscle at the level of the axillary vein; in the latissimus dorsi muscle at the level of the inferior margin of the dissection area; and in the latissimus dorsi muscle between the level of the axillary vein and the level of the inferior margin of the dissection area. All patients were female with an age range of 35–73 years (median, 49 years). Patients' height, weight, and above and below breast measurements were done before starting RT.

Postoperative RT was performed with a dose of 50 Gy (in 25 fractions) at the Department of Radiology, Keio University Hospital or Tokyo Metropolitan Hiroo Hospital. Twenty-two patients (11 with left- and 11 with right-sided breast cancer) with no, or minimal, lymphatic infiltration were treated with CTIT. CTIT was planned to irradiate the breast tissue without considering the axillary region. Figure 1a shows a simulation film, and Fig. 1b shows a patient treated

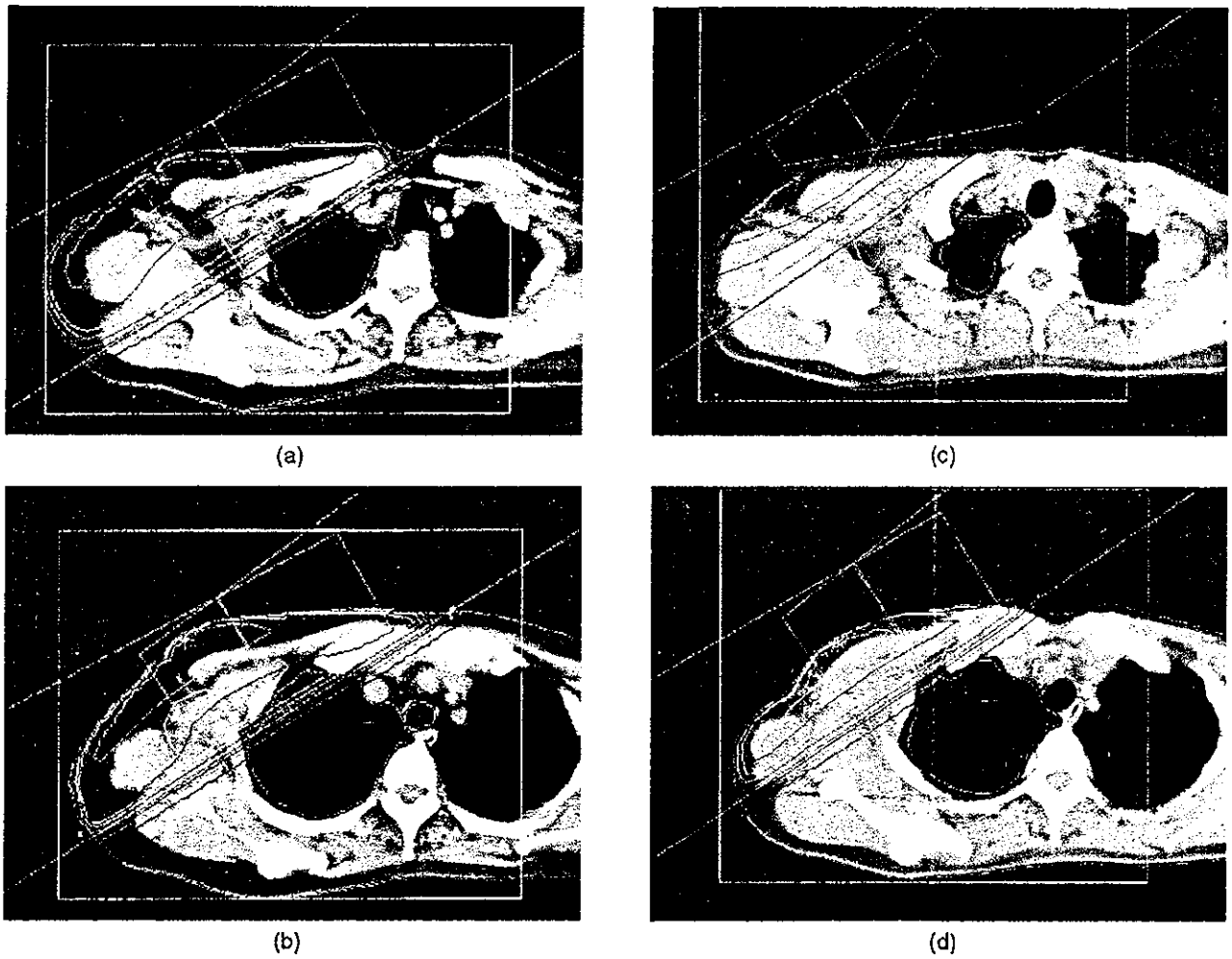

Fig. 2. Dose-distribution curve on CT slices: levels just below humeral head and axilla of patient treated with (a,b) MTIT and (c,d) CTIT. Surgical clips, seen in axillary region, were left as axillary dissection markers. White lines show limits of Levels I, II, and III. Green line is 100% isocenter dose line, blue 90%, yellow 80%, and so on.

with CTIT. The medial margin of the field was set up at the midline of the chest wall. The lateral margin was set up at the mid-axillary line. The cranial margin was 1–2 cm below the caudal edge of the humeral head. The caudal margin was 1 cm below the caudal edge of the palpable breast tissue. Twenty-two patients (14 with left- and 8 with right-sided breast cancer) with apparent lymphatic infiltration were treated with MTIT. MTIT was planned to irradiate the breast tissue and axillary region. Figure 1c shows a simulation film, and Fig. 1d shows a patient treated with MTIT. In this study, a conventional X-ray simulator was used to set the radiation field. MTIT was planned by setting the dorsal edge of the radiation field on a lateral-view simulator film at the dorsal edge of the humeral head and the cranial edge of the radiation field at the caudal edge of the humeral head, as previously reported (15). As a result, a 2–3-cm area of the humeral head was within the anterior-oblique radiation field. The collimator angle for MTIT thus had to be somewhat steeper than that of CTIT to decrease the lung volume

Table 1. Dose and volume analysis of breast, axillary regions, and lung

	MTIT (%)	CTIT (%)	95% Confidence limit
Breast			
105% dose	1–49 (22.5)	0–70 (10)	Not significant
95% dose	86–100 (96.5)	83–100 (95)	Not significant
Level I			
80% dose	79–100 (90)	1–79 (30.5)	Significant
70% dose	84–100 (94.5)	2–84 (38)	Significant
Level II			
80% dose	39–100 (81)	0–40 (8)	Significant
70% dose	59–100 (89)	0–53 (15)	Significant
Level III			
80% dose	45–100 (76)	0–20 (0)	Significant
70% dose	70–100 (89.5)	0–31 (0)	Significant
Ipsilateral lung			
90% dose	5–22 (11.5)	5–15 (9)	Significant
30% dose	12–32 (19)	10–22 (14.5)	Significant

Abbreviations: MTIT = modified tangential irradiation technique; CTIT = conventional tangential irradiation technique.
Data presented as range, with median in parentheses.

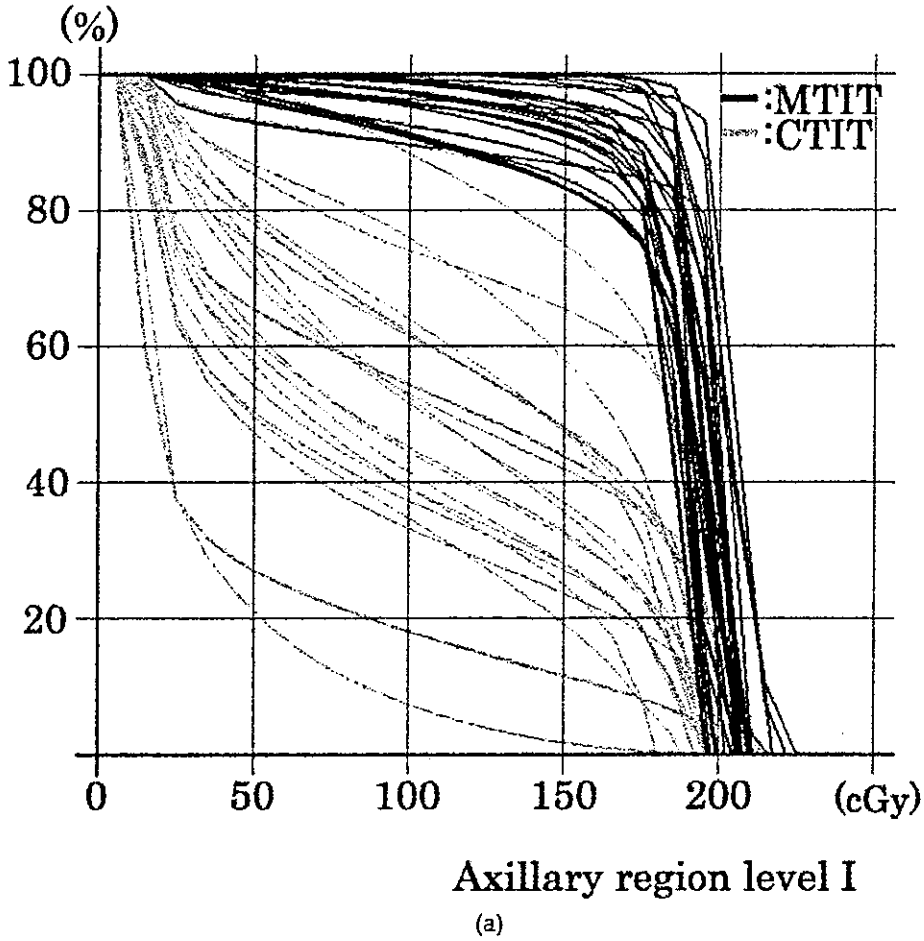

Fig. 3. DVH for patients treated with MTIT (black line) and CTIT (gray line) at (a) Level I, (b) Level II, and (c) Level III. DVHs show tolerable radiation doses at each axillary region level treated with MTIT in contrast to CTIT results.

irradiated. The medial and cranial margins were sometimes crossed over the mid-line of the chest wall.

All patients in this study underwent CT scanning with marking of the field margins and the isocenter, and the CT data were transmitted on-line to a RT planning system (FOCUS, version 2.50, Computerized Medical Systems, St. Louis, MO). The breast region was defined as the region exhibiting greater density than the surrounding fatty tissue on the CT images (displayed with a window width of 400 Hounsfield Units and a window level of 30 Hounsfield Units). The breast regions of patients >50 years, who might have had fatty degenerative changes in their breasts, were defined with 5-mm wider than margins used in other patients. Axillary lymph node regions (Levels I–III) were defined by referring to the position of the pectoralis minor muscle and the surgical clips inserted during surgery. The ipsilateral lung region was automatically defined and circumscribed by the system. The dose-distribution CT images and the DVHs for the breast, axillary lymph node region (Levels I–III), and lung were calculated for all patients. The heart volume irradiated was also calculated for the 25 patients with left-sided breast cancer.

Statistical analyses were performed using Welch's *t* test.

RESULTS

The height, weight, and above and below breast measurement for the CTIT and MTIT patients was 157.0 ± 5.0 cm and 157.0 ± 6.4 cm, 53.7 ± 5.3 kg and 54.0 ± 4.6 kg, 87.0 ± 7.0 cm and 86.6 ± 6.2 cm, and 76.8 ± 5.2 cm and 77.1 ± 5.4 cm, respectively. No differences were statistically significant between the two groups.

The dose distributions for MTIT are shown in Fig. 2a,b, and those for CTIT in Fig. 2c,d. The dose distributions on CT slices just below the humeral head level showed whole axillary regions were irradiated with MTIT; CTIT did not achieve full irradiation (Fig. 2a,c). At the CT slice level 2–3 cm below the humeral head, dorsal axillary regions were underdosed but almost the entire axillary region was covered by MTIT; however, dorsal axillary regions were not irradiated with CTIT (Fig. 2b,d).

Dose volume histogram analyses for the breast, axillary region (Levels I–III), and ipsilateral lung were performed in patients treated with MTIT and CTIT (Table 1). The breast tissue was irradiated with an 86.5–100% volume (median, 6.5%) by MTIT and 83–100% volume (median, 95%) by CTIT at >95% of the isocenter dose (Table 1). The DVHs

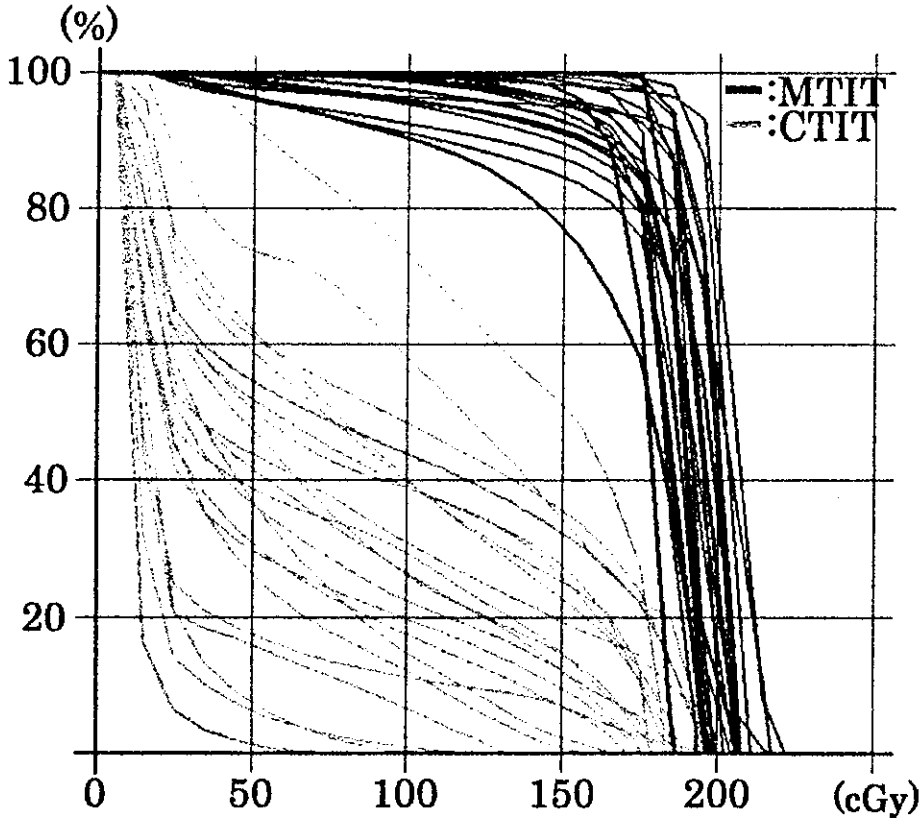

Fig. 3. (*Cont'd*).

for the axillary region Levels I, II, and III for all patients treated with MTIT and CTIT are shown in Fig. 3. DVH analyses demonstrated all axillary region levels to be well covered with MTIT compared with those treated with CTIT. The axillary lymph node regions at Levels I, II, and III were irradiated with 84–100% (median, 94.5%), 59–100% (median, 89%), and 70–100% (median, 89.5%) volumes by MTIT and 2–84% (median, 38%), 0–53% (median, 15%), and 0–31% (median, 0%) volumes by CTIT, respectively, at >70% of the isocenter dose (Table 1). The ipsilateral lung was irradiated with a 5–22% volume (median 11.5%) by MTIT and a 5–15% volume (median, 9%) by CTIT at >90% of the isocenter dose (Table 1). The irradiated dose and volume analysis of the heart for the 14 and 11 patients with left-sided breast cancer treated with MTIT and CTIT, respectively, are presented in Table 2. In all patients, the volumes irradiated with an 80% isocenter dose were <30 cm^3.

DISCUSSION

The role of routine axillary dissection in the management of localized breast cancer is controversial (1–3). Recently, early-stage breast cancer patients without clinically palpable axillary lymph nodes have reportedly been offered axillary RT without dissection (4–9). A randomized controlled study of early-stage breast cancer (National Surgical Adjuvant Breast and Bowel Project Breast-32 [NSABP B-32] is in progress, and the long-term survival and incidence of side effects will be compared between patients treated with sentinel lymph node biopsy and those receiving axillary lymph node dissection (11). Because the surgical procedures for breast cancer are smaller in scope, the radiation fields should be planned to cover wider regions. As we previously reported, it is possible to irradiate almost the entire axillary lymph node region by MTIT (15). In this study, we calculated the dose distribution and DVHs of the breast, axillary lymph node region, ipsilateral lung, and heart for all patients and demonstrated MTIT to be an adequate treatment method after breast-conserving surgery.

The breast region was defined as the area exhibiting greater density than the surrounding fatty tissue on CT. However, it is sometimes difficult to define the breast tissue in elderly patients in whom fatty degenerative change may be present in the breast. The breast region of patients >50 years old (about one-half of our patients) was determined with margins 5-mm wider than margins used in other pa-

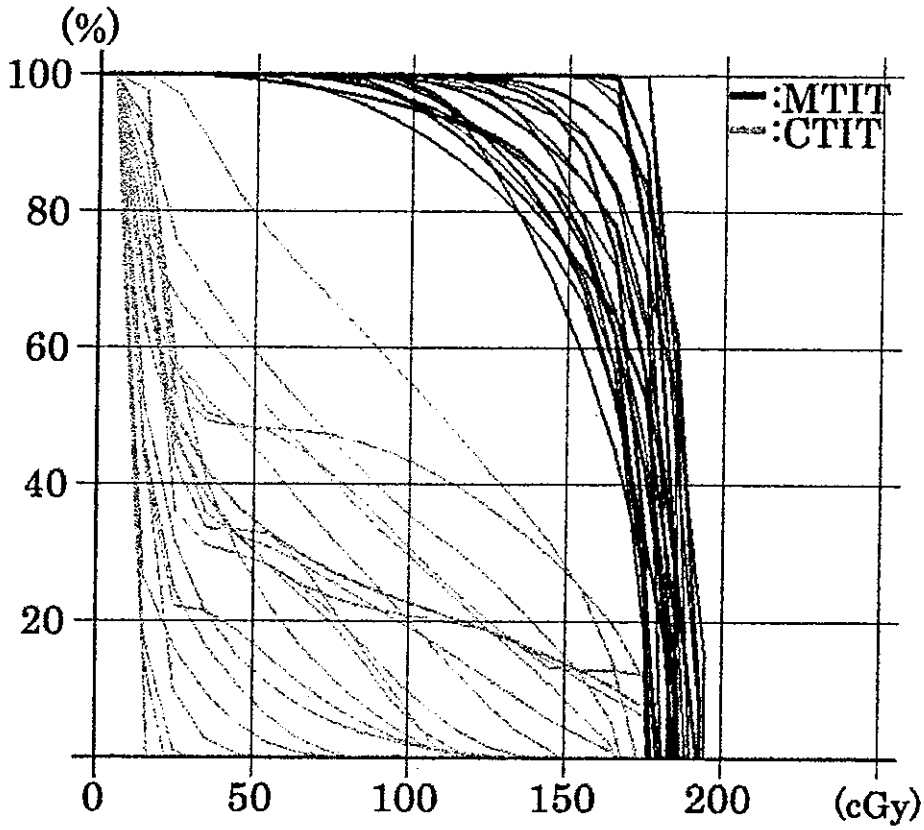

(c)

Fig. 3. (*Cont'd*).

tients. In both CTIT and MTIT planning, the breast tissue was sufficiently irradiated.

The entire axillary lymph node region, as well as the breast tissue, was irradiated by MTIT. The axillary lymph node regions at Levels I, II, and III were irradiated with 84–100% (median, 94.5%), 59–100% (median, 89%), and 70–100% (median, 89.5%) volumes, respectively, at >70% of the isocenter dose for patients treated with MTIT. The areas irradiated with MTIT at each axillary level were much wider than those irradiated with CTIT. Breast tissue is the only target in planning CTIT, and low control rates for the axillary lymph node region have generally been reported (16–18). Goodman *et al.* (19) reported the Level I area was well covered, and Aristei *et al.* (14) reported the Level I and II areas were not entirely covered by CTIT. Radiation doses of 45–50 Gy have been reported to provide excellent control rates for subclinical lymph node involvement (20). All patients in this study received 50 Gy in 25 fractions of external beam RT. Furthermore, 70% of the isocenter dose was 35 Gy (1.4 Gy/fraction), which appeared to be an insufficient dose to control axillary lymph node recurrence. However, Withers *et al.* (21) stated that the dose–response curve for control of subclinical metastases is linear, and local control of the axillary region can, to some extent, be expected at doses of <45–50 Gy. Three-dimensional conformal RT or intensity-modulated RT is anticipated to be able to handle this problem of underdosing. Long follow-up is required to determine the true benefit of MTIT.

Table 2. Irradiated heart volume in left breast cancer patients

Heart volume (cm^3)	MTIT (n = 14)			CTIT (n = 11)		
	80%	50%	30%	80%	50%	30%
0–10	13	9	6	8	5	4
11–30	1	4	6	3	4	5
31	0	1	2	0	2	2

Abbreviations as in Table 1.
Percentages represent radiation dose.

Areas near the edges of the radiation field, especially the dorsal areas at Levels I–III and the cranial areas at Levels II and III, were underdosed. Lymph node failure in the supraclavicular region, which cannot be clearly distinguished from the Level III cranial area, was seen in a few cases. However, lymph node failure in the other underdosed areas was rare. The radiation field in MTIT cannot be expanded

for dorsal direction to achieve a sufficient field margin, because the extended field would involve a larger lung volume and result in greater complication rates. Careful and accurate planning is needed at every radiation session to reduce the risk of underdosing the marginal lymph node areas and to minimize the lung volume involved.

The lung volume irradiated with MTIT was small but significantly larger than that irradiated with CTIT. Radiation pneumonitis and fibrosis have been thoroughly discussed, and reducing the lung volume irradiated must be given the highest priority to avoid these complications (22, 23). The frequency of pneumonitis varies from 0% up to 50%, depending on the radiation technique used (24–33). However, Lingos *et al.* (34) reported that the amount of irradiated lung volume was not associated with radiation pneumonitis within a limited range of irradiated lung volumes, defined as a central lung distance <3 cm. Lind *et al.* (33) reported a central lung distance >2.5 cm to be directly related to the incidence of lung complications and showed that 50% of patients had pulmonary complications with internal mammary node and supraclavicular field treatment along with the tangential breast field. We planned both CTIT and MTIT with a central lung distance of <2.5 cm and no symptomatic pulmonary complications had occurred at 1 year after treatment.

Rutqvist *et al.* (35, 36) reported a high dose of ^{60}Co radiation to be associated with a high risk of cardiac complications. However, when an electron beam was used for the internal mammary node field, no complications occurred. It was concluded that cardiac problems could be avoided by the use of proper field arrangements and reducing the radiation dose. In this series, the irradiated heart volume was negligible in right-sided breast cancer patients and was also very small in left-sided breast cancer patients. Cardiac toxicity would not be produced by MTIT, as reported for CTIT (32, 37).

CONCLUSION

Our results suggest that the breast tissue was sufficiently irradiated with both CTIT and MTIT planning, that axillary lymph node areas irradiated by MTIT were much wider than those irradiated by CTIT at all levels, that the lung and heart volumes irradiated by MTIT were small, and that pulmonary and cardiac toxicity may not be increased compared with the results reported thus far.

REFERENCES

1. Cady B. The need to reexamine axillary lymph node dissection in invasive cancer. *Cancer* 1994;73:505–508.
2. Haffty BG, Ward B, Pathare P, *et al.* Reappraisal of the role of axillary lymph node dissection in the conservative treatment of breast cancer. *J Clin Oncol* 1997;15:691–700.
3. Dent DM. Axillary lymphadenectomy for breast cancer: Paradigm shifts and pragmatic surgeons. *Arch Surg* 1996;131: 1125–1127.
4. Cady B, Stone MD, Wayne J. New therapeutic possibilities in primary invasive breast cancer. *Ann Surg* 1993;218:338–349.
5. Halverson KJ, Taylor ME, Perez CA, *et al.* Regional nodal management and patterns of failure following conservative surgery and radiation therapy for stage 1 and 2 breast cancer. *Int J Radiat Oncol Biol Phys* 1993;26:593–599.
6. Hoskin PJ, Rajan B, Ebbs S, *et al.* Selective avoidance of lymphatic radiotherapy in the conservative management of early breast cancer. *Radiother Oncol* 1992;25:83–88.
7. Kuznetsova M, Graybill JC, Zusag TW, *et al.* Omission of axillary nymph node dissection in early-stage breast cancer: Effect on treatment outcome. *Radiology* 1995;197:507–510.
8. Ogawa Y, Nishioka A, Inomata T, *et al.* Conservation treatment intensified with tamoxifen and CAF chemotherapy without axillary dissection cancer patients with clinically-negative axillary nodes. *Oncol Rep* 1999;6:801–805.
9. Wong JS, Recht A, Beard CJ, *et al.* Treatment outcome after tangential radiation therapy without axillary dissection in patients with early-stage breast cancer and clinically negative axillary nodes. *Int J Radiat Oncol Biol Phys* 1997;39:915–920.
10. Harlow SP, Krag DN. Sentinel lymph node—Why study it: Implications of the B-32 study. *Semin Surg Oncol* 2001;20: 224–229.
11. Muren LP, Maurstad G, Hafslund R, *et al.* Cardiac and pulmonary doses and complication probabilities in standard and conformal tangential irradiation in conservative management of breast cancer. *Radiother Oncol* 2002;62:173–183.
12. Hong L, Hunt M, Chui C, *et al.* Intensity-modulated tangential beam irradiation of the intact breast. *Int J Radiat Oncol Biol Phys* 1999;44:1155–1164.
13. Kong FM, Klein EE, Bradley JD, *et al.* The impact of central lung distance, maximal heart distance, and radiation technique on the volumetric dose of the lung and heart for intact breast radiation. *Int J Radiat Oncol Biol Phys* 2002;54:963–971.
14. Aristei C, Chionne F, Marsella AR, *et al.* Evaluation of level I and II axillary nodes included in the standard breast tangential fields and calculation of the administered dose: Results of a prospective study. *Int J Radiat Oncol Biol Phys* 2001;51:69–73.
15. Takeda A, Shigematsu N, Kondo M, *et al.* The modified tangential irradiation technique for breast caner: How to cover the entire axillary region. *Int J Radiat Oncol Biol Phys* 2000; 46:815–822.
16. Krasin M, McCall A, King S, *et al.* Evaluation of a standard breast tangent technique: A dose-volume analysis of tangential irradiation using three-dimensional tools. *Int J Radiat Oncol Biol Phys* 2000;47:327–333.
17. Smitt MC, Goffinet DR. Utility of three-dimensional planning for axillary node coverage with breast-conserving radiation therapy: Early experience. *Radiology* 1999;210:221–226.
18. Botnick M, McCormick Hunt M, *et al.* Are the axillary lymph nodes treated by standard tangent breast fields? [Abstract]. *Int J Radiat Oncol Biol Phys* 1998;42:245.
19. Goodman RL, Grann A, Saracco P, *et al.* The relationship between radiation fields and regional lymph nodes in carcinoma of the breast. *Int J Radiat Oncol Biol Phys* 2001;20:99–105.
20. Montague ED, Tapley ND, Baker JL. Radiotherapy in the management of nondisseminated breast cancer. In: Fletcher GH, editor. Textbook of radiotherapy, 3rd ed. Philadelphia: Lea & Febiger, 1980: p. 527–579.
21. Withers HR, Peters LJ, Taylor JMG. Dose-response relationship for radiation therapy of subclinical disease. *Int J Radiat Oncol Biol Phys* 1995;31:353–359.
22. Hardman PD, Tweeddale PM, Kerr GR, *et al.* The effect of

pulmonary function of local and loco-regional irradiation for breast cancer. *Radiother Oncol* 1994;30:33–42.
23. Kimsey FC, Mendenhall NP, Ewald LM, *et al.* Is radiation treatment volume a predictor for acute and late effect on pulmonary function? A prospective study of patients treated with breast-conserving surgery and postoperative irradiation. *Cancer* 1994;73:2549–2555.
24. Read PE, Ash DV, Thorogood J, *et al.* Short term morbidity and cosmesis following lumpectomy and radical radiotherapy for operable breast cancer. *Clin Radiol* 1987;38:371–373.
25. Rothwell RI, Kelly SA, Joshlin CAF. Radiation pneumonitis in patient treated for breast cancer. *Radiother Oncol* 1985;4: 9–14.
26. Lind BK, Brahme A. Optimization of radiation therapy dose distributions using scanned electron and photon beams and multileaf collimators. In: Bruinvis IAD, van der Giessen PH, van Kleffens HJ, Wittkämper FW, editors. Proceedings of the Ninth International Conference on the Use of Computers in Radiation Therapy. Scheveningen, The Netherlands; 1987. p. 227–330.
27. Rotstein S, Lax I, Svane G. Influence of radiation therapy on the lung tissue in breast cancer patients: CT-assessed density changes and associated symptoms. *Int J Radiat Oncol Biol Phys* 1990;18:173–180.
28. Polansky SM, Ravin CE, Prosnitz LR. Pulmonary changes after primary irradiation of early breast carcinoma. *AJR Am J Roentgenol* 1980;134:101–105.
29. Halverson KJ, Leung TC, Pellet JB, *et al.* Study of treatment variation in radiotherapy of head and neck tumors using a fiber-optic radiotherapy imaging system. *Int J Radiat Oncol Biol Phys* 1991;21:1327–1336.
30. Markiewicz DA, Scultz DJ, Haas JA, *et al.* The effects of sequence and type of chemotherapy and radiation therapy on cosmesis and complications after breast conservation therapy. *Int J Radiat Oncol Biol Phys* 1996;35:661–668.
31. Pierce SM, Recht A, Lingos TI, *et al.* Long-term radiation complications following conservative surgery (CS) and radiation therapy (RT) in patients with early stage breast cancer. *Int J Radiat Oncol Biol Phys* 1992;23:915–923.
32. Fowble B, Fein DA, Hanlon AL, *et al.* The impact of tamoxifen on breast recurrence, cosmesis, complications, and survival in estrogen receptor-positive early-stage breast cancer. *Int J Radiat Oncol Biol Phys* 1996;35:669–677.
33. Lind PARM, Gagliardi G, Wennberg B, *et al.* A descriptive study of pulmonary complications after postoperative radiation therapy in node-positive stage II breast cancer. *Acta Oncol* 1997;36:509–515.
34. Lingos TI, Recht A, Vicini F, *et al.* Radiation pneumonitis in breast cancer patients treated with conservative surgery and radiation therapy. *Int J Radiat Oncol Biol Phys* 1991;21:355–360.
35. Rutqvist LE, Johansson H. Mortality by laterality of primary tumour among 55 000 breast cancer patients from Swedish cancer registry. *Br J Cancer* 1990;61:866–868.
36. Rutqvist LE, Lax I, Fornander T, *et al.* Cardiovascular mortality in randomized trial of adjuvant radiation therapy versus surgery alone in primary breast cancer. *Int J Radiat Oncol Biol Phys* 1992;22:887–896.
37. Das IJ, Cheng EC, Freedman G, *et al.* Lung and heart dose volume analyses with CT simulator in radiation treatment of breast cancer. *Int J Radiat Oncol Biol Phys* 1998;42:11–19.

ELSEVIER

Radiotherapy and Oncology 70 (2004) 45–48

RADIOTHERAPY & ONCOLOGY

www.elsevier.com/locate/radonline

Technical note

Measurement of beam-axis displacement from the isocenter during three-dimensional conformal radiosurgery with a micro-multileaf collimator

Etsuo Kunieda[a,*], Osamu Kawaguchi[a], Hidetoshi Saitoh[a,b], Tatsuya Fujisaki[a,c], Atsuya Takeda[a], Takatsugu Kawase[a], Hossain M. Deloar[a,d], Naoyuki Shigematsu[a], Atsushi Kubo[a]

[a]*Department of Radiology and Neurosurgery, Keio University, 35 Shinanomachi, Shinjuku, Tokyo 160-8582, Japan*
[b]*Department of Radiologic Sciences, Tokyo Metropolitan University of Health Sciences, Tokyo, Japan*
[c]*Department of Radiological Sciences, Ibaraki Prefectural University of Health Sciences, Ibaraki, Japan*
[d]*Japan Science and Technology Agency, Japan*

Received 20 March 2003; received in revised form 7 November 2003; accepted 17 November 2003

Abstract

We describe the displacement of the beam-axis from the planning isocenter in clinical situations during three-dimensional conformal radiosurgery using an Acculeaf bi-directional micro-multileaf collimator. The displacements were recorded for 64 ports using a video imaging system and a stereotactic arc. The mean displacement was 0.41 ± 0.25 mm.
© 2003 Elsevier Ireland Ltd. All rights reserved.

Keywords: Accuracy; Linear accelerator; Radiosurgery; Beam's eye monitor

1. Introduction

Recently, micro-multileaf collimators (MMLC) have been used for radiosurgery or precise three-dimensional (3D) conformal radiotherapy [2,4,5,8,9]. Nevertheless, the majority of medical linear accelerators (linacs) currently in operation are not designed to be used with heavy auxiliary MMLC hardware. Moreover, as a result of the patient's head and the couch interfering with placement of the film, verification of each actual treatment port is very difficult or practically impossible to carry out during 3D-conformal radiotherapy or radiosurgery. Most of the previously reported measurements were not carried out during treatment, but instead, were taken in phantom studies [3,6,7].

We report a method to evaluate the degree of error during MMLC-based radiosurgery and indicate the displacement of the beam-axis from the planning isocenter during this procedure in clinical situations.

2. Materials and methods

A 6-MV linac (ML15MV: Mitsubishi Electric Corp. Tokyo, Japan) was used to produce the X-ray beam. This machine has been used for the last 8 years for radiosurgery in addition to daily conventional irradiation. During radiosurgery or stereotactic radiotherapy with this linac, a computer-controlled MMLC module (AccuLeaf: Alayna Enterprises Corporation, Paris, France) was mounted on the linac gantry-head. Forty-eight pairs of MMLC leaves, driven by individual motors, are composed of two levels with the direction of the two levels of leaves being perpendicular to each other. The effective leaf thickness of the inner 14 pairs is 2.6 mm, while the thickness of the outer pairs is 5.3 mm at the isocenter [1]. The outer dimensions of the MMLC are 540 mm in diameter and 135 mm in height with a weight of 28 kg (Fig. 1).

For the purpose of target positioning, we have been using a small charge-coupled device (CCD) video camera mounted in the gantry head where the source of the light field is placed (beam's eye monitor). Details were described elsewhere [6]. During each treatment or QA procedure, a stereotactic arc is mounted on the base frame in such a way that the center of the arc can be matched with the intended target point (i.e. the planning isocenter). A target pointer, consisting of a convex lens and a bull's eye, can slide along the arc with its axis perpendicular to the arc. If we observe the bull's eye through the lens from the video camera, the lens forms a virtual image of the bull's eye ('virtual target') at the position of the arc center (planning isocenter), even

* Corresponding author.

0167-8140/$ - see front matter © 2003 Elsevier Ireland Ltd. All rights reserved.
doi:10.1016/j.radonc.2003.11.008

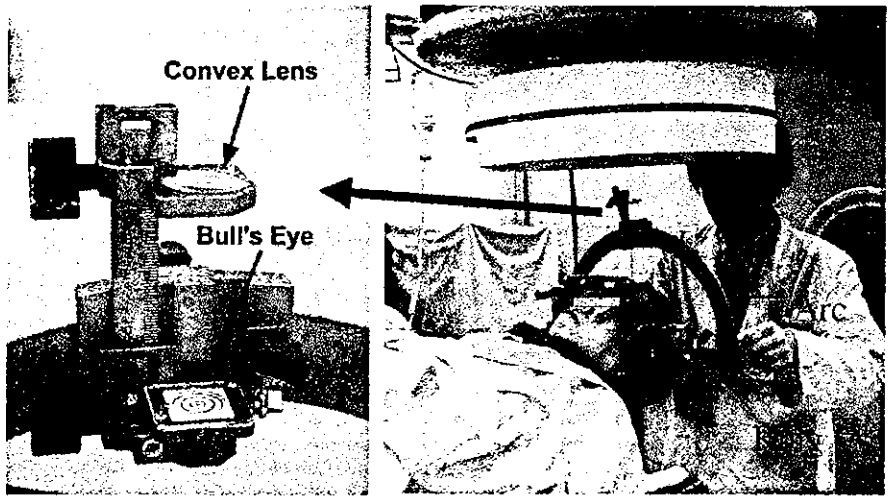

Fig. 1. The micro-multileaf collimator (MMLC) module and the stereotactic arc device (right). Mounted on the arc is a target pointer, consisting of a convex lens and a bull's eye (left).

though the actual position of the bull's eye is far away from the center. Since the virtual target is 'located' at the center of the arc, the position is stable as long as we observe the image of the bull's eye through the lens.

Although this mechanism was developed originally for target positioning during circular collimator-based radiosurgery, we integrated it using in-house software for quantitative analysis of beam displacement. The calibration for determining the center of the beam's eye image was also carried out for the measurement each time prior to treatment of a patient. To indicate actual distances at the isocenter, concentric circles were prepared on the bull's eye of the target indicator so that each circle represented displacement in millimeters. That is, the virtual image of the concentric circles was located at the isocenter, with the diameter of the innermost circle being 1 mm. The distances in the beam's eye image and actual shifts from the isocenter were compared and verified by application of conversion software.

A tungsten ball of 4 mm diameter was used to confirm the agreement between the beam's eye monitor and the irradiation field. The ball was first placed near the isocenter of the linac using wall-mounted laser beams. It was not necessary to position the ball precisely at the true 'isocenter' of the machine. Instead it was positioned at a temporarily defined 'isocenter' that was eventually corrected by the iterative procedure described below. The ball was used only for calibration purposes for the monitor system and not used directly for target positioning.

The tungsten ball fixed at the temporary isocenter was observed through the beam's eye monitor at gantry angles of both 0 and 180°. The position of the ball in both beam's eye images was measured on the computer screen. If both positions were the same, the ball was considered to be at the isocenter, or at least at an isocentric point in the plane of gantry rotation. Alternatively, if the position of the center of the ball was different in both images, then the midpoint was defined as the second temporary isocenter. The third or fourth temporary isocenter was decided by the same procedure, until the position of the ball was stabilized. The position of the ball at the isocenter was finally confirmed with continuous observation of the beam's eye monitor during 360° rotation of the gantry.

With the above procedure, only the position of the ball in the plane of gantry rotation was aligned with the isocenter. Therefore, similar adjustments were carried out using the collimator rotation mechanism of the linac gantry-head. This calibration procedure was completed with real-time monitoring of the beam's eye image displayed on the computer screen, thereby eliminating the need to leave the treatment room to avoid X-ray exposure. This adjustment of the isocenter could be carried out within 5 min. Finally, after defining the 'isocenter', alignment of both the axis of the X-ray beam and the beam's eye monitor was confirmed using X-ray film exposure of the tungsten ball. The 'center' of the beam's eye image was also confirmed from the position of the center of the tungsten ball in the image, with the 'center' being used for subsequent measurements of beam-axis displacement.

2.1. Measurement of beam-axis displacement

During the treatment, before each fixed-beam irradiation, the position of the virtual target was observed and recorded. Five consecutive radiosurgery cases involving a total of 64 irradiation fields were analyzed for this study. The patients' heads were fixed in a Leksell stereotactic frame with screws. After the couch and gantry settings had been established for each field of irradiation, the stereotactic arc was rotated, and

the target indicator was moved along the arc so that the virtual image of the bull's eye could be seen through the lens. The image of the beam's eye monitor was then recorded. For reference, images were also recorded at a couch angle of zero, with a gantry angle of 0, ±90°, and at couch angles of −45, +45, and +90° with a gantry angle of 0. The distances from the 'center' of the beam's eye image to the position of the bull's eye were then measured.

According to our protocol, when the error was greater than 0.7 mm, the position of the patient was corrected with a horizontal movement of the couch. Nevertheless, the data of the displacement that we used for further analysis were those obtained before this correction.

The stereotactic arc with the target indicator was kept on the frame during the treatment but not left in the radiation field with the arc being rotated and usually kept in the most downward position during irradiation. Less than 1 min was required to measure the displacement for each beam.

3. Results

The displacements of the beam-axis from the center of the arc are shown in Fig. 2. The mean displacement (±SD) was 0.41 ± 0.25 (range 0–0.99) mm for all measurements. For 25 measurements, when the couch angle was zero, the mean displacement was 0.16 ± 0.12 (0–0.44) mm (Fig. 2a), whereas for 39 measurements with non-zero couch angles, the displacement was 0.56 ± 0.24 (0.14–0.99) mm. Among non-zero couch angles, for absolute couch angles greater than 40° (33 measurements) and ≤40° (six measurements), the displacements were 0.61 ± 0.24 (0.14–0.85) mm and 0.32 ± 0.09 (0.22–0.50) mm, respectively.

To clarify the contribution of gantry rotation to the displacements, 25 measurements with the couch angle position at 0° were used. The contributions of the displacement attributable to gantry rotation were then examined (Fig. 2b). In this subset of measurements, the displacements were 0.09 ± 0.04 (0–0.14) mm when the gantry head was in upper positions (i.e. from −50 to 50°: 13 measurements), and 0.26 ± 0.11 (0.12–0.44) mm when the gantry head was at lateral positions (at an angle greater than 50° from the top on either side: 12 measurements). The maximum displacement for couch angle 0 was 0.44 mm and found at gantry angle of 114° (clockwise rotation). For six measurements with both couch and gantry angles equal to zero, the displacement was 0.07 ± 0.06 (0–0.14) mm. The displacements were greater than 0.7 mm in 12 of the 64.

4. Discussion

Although our positioning mechanism was developed primarily for target positioning in radiosurgery [6], we employed it to verify the isocentric accuracy of each beam

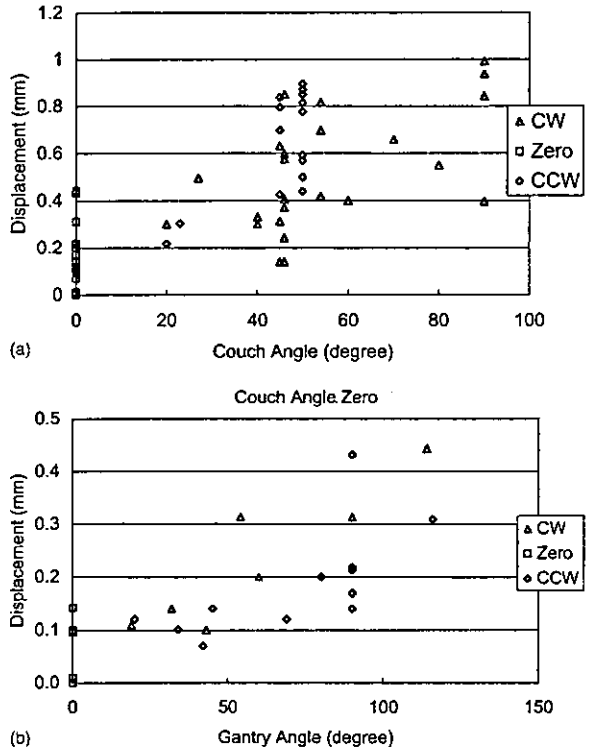

Fig. 2. (a) Couch angle (absolute value) and the displacements of the beam-axis from the planning isocenter. CW, clockwise rotation of the couch; CCW, counter-clockwise rotation; Zero, couch angle of zero. (b) Gantry angle (absolute value) and the displacements of the beam-axis from the planning isocenter for 25 measurements performed at the couch angle of zero. CW, clockwise rotation of the gantry; CCW, counter-clockwise rotation; Zero, gantry angle of zero.

during fixed-beam radiosurgery with an MMLC. The major advantages of using this mechanism for verification are as follows.

1. The verification of geometric accuracy can be obtained even when the patient's head is placed at the isocenter.
2. The verification is available while the gantry and couch are in a rotated position.
3. Correction of the patient's position can be carried out immediately by referring to the real-time images, without the need for X-ray exposures.

In reality, there are many factors that affect beam-axis deviation from the intended target. Even after positioning of the patient's head is completed, some degree of misalignment of the planning isocenter and the beam-axis may occur, as a result of unintended stress to the patient's head or mechanical error of the machine.

Our measurements indicated more than 0.7 mm shift of the planning isocenter from the mechanical isocenter in 12 out of 64 ports, and we corrected the displacement for each fixed-port irradiation. These shifts were larger than values

we obtained in our previous study [6] and also those reported in other phantom studies [3,7]. This discrepancy could be due to the fact that our current measurements were carried out during treatment while using an additional MMLC collimator. The displacements were large when the angle of rotation of the couch was non-zero. This is possibly as a consequence of wobbling and excursion of the couch rotation-axis from the 'true' isocenter, and this deviation is often difficult to correct once the machine has been installed. When arc irradiations are employed for radiosurgery or when port-by-port correction is not available, the horizontal position of the couch should be moved and corrected at each rotational angle to avoid the inaccuracy caused by rotation of the couch. From our data and other investigations, displacement of the beam-axis from the 'isocenter' depends on the gantry rotational angle [3,7]. This displacement can be explained by gravitational bending of the gantry head due to its weight, and in order to minimize this effect the range of gantry rotation should be limited. We recommend aligning the beam-axis to the mechanical isocenter for each port, or at least at each couch rotation, when a high degree of accuracy is required for each beam delivery.

References

[1] Bucciolini M, Russo S, Banci Buonamici F, Pini S, Silli P. Dosimetric characterization of a bi-directional micromultileaf collimator for stereotactic applications. Med Phys 2002;29:1456–63.
[2] Cosgrove VP, Jahn U, Pfaender M, Bauer S, Budach V, Wurm RE. Commissioning of a micro multi-leaf collimator and planning system for stereotactic radiosurgery. Radiother Oncol 1999;50:325–36.
[3] Gibbs FJ, Buechler D, Leavitt DD, Moeller JH. Measurement of mechanical accuracy of isocenter in conventional linear-accelerator-based radiosurgery. Int J Radiat Oncol Biol Phys 1993;25:117–22.
[4] Grebe G, Pfaender M, Roll M, Luedemann L, Wurm RE. Dynamic arc radiosurgery and radiotherapy: commissioning and verification of dose distributions. Int J Radiat Oncol Biol Phys 2001;49:1451–60.
[5] Kubo HD, Pappas CT, Wilder RB. A comparison of arc-based and static mini-multileaf collimator-based radiosurgery treatment plans. Radiother Oncol 1997;45:89–93.
[6] Kunieda E, Kitamura M, Kawaguchi O, et al. New system for linear accelerator radiosurgery with a gantry-mounted video camera. Int J Radiat Oncol Biol Phys 1998;40:739–46.
[7] Lutz W, Winston KR, Maleki N. A system for stereotactic radiosurgery with a linear accelerator. Int J Radiat Oncol Biol Phys 1988;14:373–81.
[8] Schlegel W, Pastyr O, Bortfeld T, et al. Computer systems and mechanical tools for stereotactically guided conformation therapy with linear accelerators. Int J Radiat Oncol Biol Phys 1992;24:781–7.
[9] Shiu AS, Kooy HM, Ewton JR, et al. Comparison of miniature multileaf collimation (MMLC) with circular collimation for stereotactic treatment. Int J Radiat Oncol Biol Phys 1997;37:679–88.